ACADEMIC PRESS

Available online at www.sciencedirect.com

SCIENCE DIRECT®

Journal of Sound and Vibration 262 (2003) 591–611

JOURNAL OF SOUND AND VIBRATION

www.elsevier.com/locate/jsvi

Equilibrium point damage prognosis models for structural health monitoring

Rebecca L. Brown, Douglas E. Adams*

School of Mechanical Engineering, Purdue University, Ray W. Herrick Laboratories, 180 S. Intramural Dr., West Lafayette, IN 47907-2031, USA

Received 28 September 2001; accepted 15 October 2002

Abstract

Most structural dynamic systems are of high order; however, they often exhibit phenomena that can be dealt with effectively using low order models. This paper presents a method for describing certain kinds of damage evolution in mechanical systems. The method relies on a simple principle that as damage evolves in a structural dynamic system, the damage indicator (i.e., diagnostic feature) behaves like a stable quasi-stationary equilibrium point in a subsidiary non-linear bifurcating system within the so-called damage center manifold. It is shown that just as linear normal modes govern the behavior of linear structures with idealized damping, so too do non-linear normal forms govern the evolution of damage within structures in many instances. The method is justified with citations from the literature on certain types of mechanical failure and then applied in an experimental case involving reversible damage in a bolted fastener. Off-line experiments on a rotorcraft fuselage show that the evolution of damage is sensitive to both temporal and spatial bifurcation parameters. A diagnostic sensing strategy whereby output-only transmissibility features are used to decrease the order of high order structural dynamic measurements is also described.

1. Introduction

1.1. Motivation

Although structural diagnosis (i.e., detection, location, and quantification of damage) continues to be an important area for basic research and development, damage prognosis has emerged as the next critical challenge in structural health monitoring (SHM) and non-destructive evaluation (NDE) [1]. These technologies for condition-based maintenance are good alternatives in many

*Corresponding author. Tel.: +1-765-496-6033; fax: +1-765-494-0787.
E-mail address: deadams@ecn.purdue.edu (D.E. Adams).

0022-460X/03/$ - see front matter
doi:10.1016/S0022-460X(03)00113-5

instances to manual inspection, which is time consuming and prone to error. Furthermore, SHM approaches are a promising means for identifying certain types of damage like barely visible impact damage (BVID) that is sometimes introduced into structures during routine service and maintenance operations, and multi-site corrosion fatigue (MCF), which both occur with increasing frequency due to the escalating use of hybrid structures in advanced multi-component heterogeneous systems (see Refs. [2,3]). New methods must be developed to describe and predict how damage evolves in structures like this before their reliability can be accurately forecasted in near real-time.

Thorough prognoses must be made before transportation or defense-related systems are taken out of commission temporarily for service and maintenance. For example, airlines cannot afford to make decisions based on overly conservative aircraft health monitoring systems because certain types of deterioration naturally occur before aircraft are ordinarily serviced [4]. Moreover, structural systems like the Comanche and Apache rotorcraft as discussed by Walsh et al. [5] and Baker [6], and Army missile systems described by Vandiver [7] cannot be grounded unnecessarily because they are critical to the success of military missions. In applications like these, false alarms must be avoided, and then diagnoses must be followed-up with accurate prognoses to optimize utility and preempt catastrophic failures. The ultimate goal is to reduce life-cycle costs, enhance supportability, and prevent human injury.

Fig. 1 illustrates how condition-based maintenance in the form of either SHM or NDE helps to individualize service schedules for systems with limited design lives when the operating environments vary from mild to more severe. The role of diagnosis is to detect damage and monitor its progression, whereas prognosis determines the rate at which damage accumulates towards failure. This information is used to optimize maintenance schedules for safety and cost. The state-of-the-art in SHM/NDE give operators information about damage but rarely produce accurate prognoses because diagnostic features are measurable and are often largely independent of the kind of system being monitored, whereas prognostics depend significantly on the system's operating environment under investigation and the material/structural constitutive behavior. Metals, metal composites, ceramics, heterogeneous materials in polymer matrix composites, and

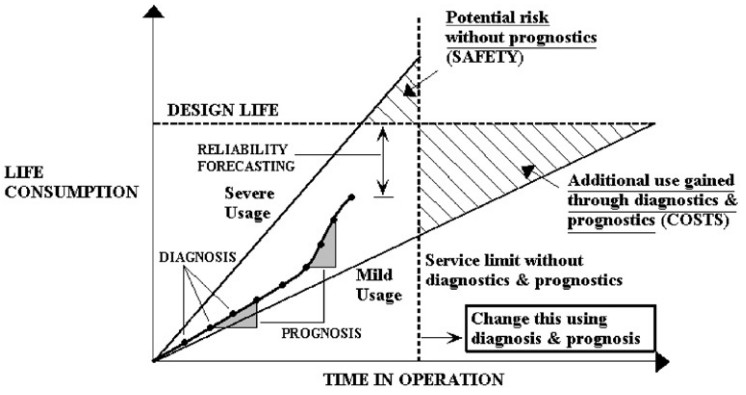

Fig. 1. Illustration of structural diagnosis and prognosis and the potential economic/safety benefits of real-time SHM as adopted from Ref. [8].

common fasteners, for example, fail in different ways at different rates. The challenge in damage prognosis is to model and predict damage accumulation in hybrid structures and systems with different kinds of damage mechanisms and failure modes (e.g., cracks, delamination, fastener failure, corrosion fatigue, etc.).

1.2. Key assumptions

The development below makes several assumptions. First, it focuses on SHM approaches rather than NDE techniques because damage is often most easily observed in operation under dynamic loading and SHM can assess structural integrity in near real-time in operating environments of varying severity. For example, fatigue cracks in metals and delaminations in composites open and close when subjected to operating stresses but are completely closed off-line [5]. Second, it assumes that a diagnostic feature, which is representative of the failure mode of interest, is measurable or at least observable. Vibration-based damage-identification features can be selected from a set of time-domain autoregressive exogenous (ARX) model coefficients, frequency-domain input–output impedance or output-only transmissibility measurements, or any other type of operating response measurement [9]. This paper assumes that sensors are available to measure the diagnostic indicator of interest even if the damage takes place over varying spatial scales (e.g., structures, volume elements, macro-cracks, and micro-defects; see Ref. [10]). Several sensing strategies exist for measuring local and global in-plane and out-of-plane response including optical fibers with Bragg gratings examined by Chang et al., Matrat et al. and others [11,12], embedded polymer-based piezoelectric composites developed by Blanas et al. [13,14], and standard PKI zirconate titanate (PZT) for actuation and sensing implemented by Wang and Chang [15] and others.

The third assumption is that sufficient SHM diagnostic data is available to develop a phenomenological, not physics-based, description of the evolving damage. The damage of interest must evolve at a slow enough initial rate to provide a database of diagnostic features, which can then be modelled as described below. A phenomenological approach has the advantage that it is viable for (theoretically) all types of materials and heterogeneous/hybrid structures, but has the disadvantage that it is largely empirical in nature.

Fourth, and most importantly, the approach below assumes that, even though structures are of high order with many global and local modes of vibration, the initiation and evolution of structural damage can be adequately described with a subsidiary low-order non-linear dynamic model. The paper postulates that as the structure is operated and vibrates, damage actually evolves on a lower dimensional ('center') manifold according to a non-linear normal form bifurcation [16]. This low order evolution of damage occurs in parallel with the dynamics of the structural system. Fig. 2 illustrates this assumption, which is the basis for the approach to be developed in Section 3. The evolution of two different types of damage to failure, a growing crack and a loosening fastener, is modelled with the same first order non-linear differential equation.

The key to this approach is to equate levels of damage with equilibrium points in subsidiary non-linear dynamic systems. This approach is justified because bifurcations [17], like damage, cause qualitative changes in a system's dynamics. In fact, SHM techniques use changes in the structural response to diagnose damage. As damage initiates and evolves, new equilibrium points are created/destroyed and move in pseudo-steady fashion along a surface in parameter space.

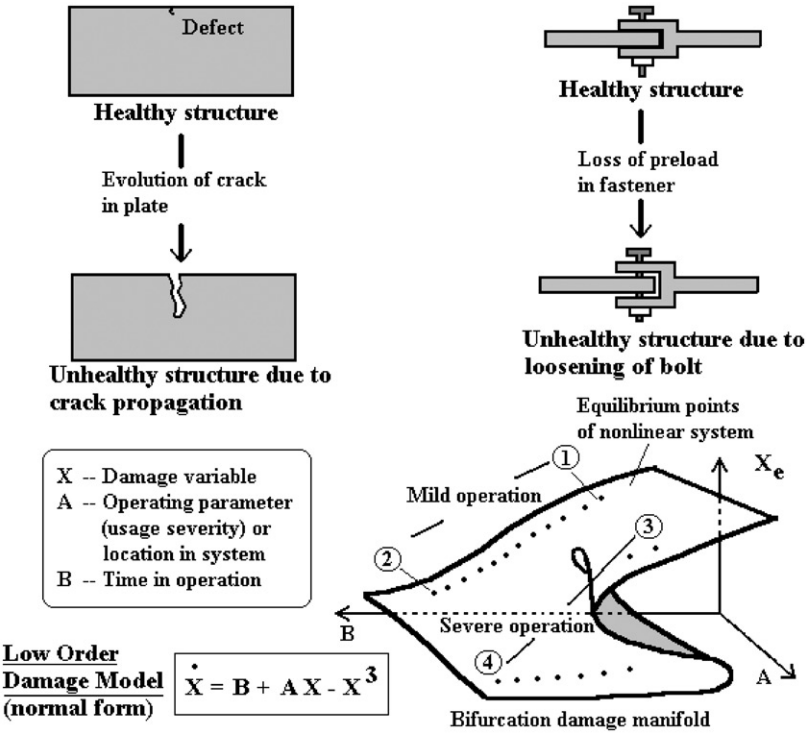

Fig. 2. Illustrations of normal forms for describing bifurcation damage in structures.

When a system follows the path from points 1 to 2, the evolution model describes a gradual change in the damage state; however, the path from points 3 to 4 indicates that the damage state changes suddenly (catastrophic). The objective of prognosis is to extract damage features from input–output or output-only data, model the evolution of those damage features using a low order dynamic system (e.g., first order system in Fig. 2), and predict the future evolution of damage through extrapolation on the manifold of damage equilibrium points. This paper develops the theory for this approach and applies it in a reversible damage experiment. The technique can only be validated through application in numerous real-world damage scenarios.

1.3. Literature review and state-of-the-art

Most previous research in damage prognosis, failure analysis, and life prediction has been largely empirical and statistical in nature (see Refs. [18,19] for instance). For instance, Weibull distributions are a popular model in machinery prognostics; however, these models assume that the operating environment is stationary. In many applications (e.g., defense and civil infrastructure), this assumption may not be valid as operating environments change frequently. In support of the fourth assumption above, Hart-Smith [20,21] showed that disbonds in adhesive composites can undergo catastrophic (sudden) unzipping, self-arrest tantamount to flattening of the damage surface in Fig. 2, or low-cycle peeling failures, all of which can be described with a

single low order non-linear model. Other failures of composite materials cited in the literature [22] also seem to be well described by low order models. Much of the previous research in bifurcation theory has been conducted in the controls community. For example, Moon [23] discusses a subcritical Hopf bifurcation in a system with fluid–structure interactions, and Namachchivaya discusses a system with a codimension two bifurcation [24]. The work discussed here using bifurcation theory in the area of experimental damage prognosis appears to be relatively new and unexplored in the structural dynamics/smart structures communities.

Section 2 begins by briefly describing how a transmissibility-based diagnostic technique is chosen to describe the progression of structural damage and is used to reduce the dimension of structural dynamic response measurements onto a so-called damage center manifold. A multiple degree-of-freedom (d.o.f.) simulation of a fastener failure is used to demonstrate this diagnostic technique. Section 3 introduces the theory for the low-order non-linear damage modelling concept. Then the damage prognosis approach is applied to experimental data from a rotorcraft fuselage in Section 4 and conclusions are given in Section 5.

2. Diagnosing damage in structures

2.1. Transmissibility for order reduction

This first step towards prognosis is diagnosing the damage state (Fig. 1). The goal of structural diagnostics in general is to extract features from input–output or output-only measurements to describe the deterioration or damage state. Although NDE is absolute in nature, basing its diagnosis on a single measurement, SHM bases its diagnoses on a history of such measurements. The focus of local vibration-based diagnostics is to reduce the dimension of the measurement(s) by extracting low order features that describe the accumulation of damage. Before introducing the damage prognosis modelling technique, transmissibility-based diagnostics are discussed in the context of data reduction and feature extraction. Refer to Johnson and Adams [25] for details on this technique.

Fig. 3 shows a typical structural dynamic system with a bolted fastener. The bolt could also represent a rivet, adhesive, or laminated joint. D.o.f.s 1 and 2 represent the bulk of the structure, the linear stiffness and damping K_{23} and C_{23} represent the fastener coupling of interest, and d.o.f. 3 represents the remainder of the structure (not constrained in this case). K_{23} can either represent a linear stiffness when the bolt is preloaded, or a clearance/gap non-linearity if the preload vanishes completely. Assuming the structural dynamic system admits a lumped parameter description, the model in Fig. 3(b) is valid and the equations of motion for a linear joint stiffness, K_{23}, are

$$[\mathbf{M}]\{\ddot{\mathbf{x}}(t)\} + [\mathbf{C}]\{\dot{\mathbf{x}}(t)\} + [\mathbf{K}]\{\mathbf{x}(t)] = \{\mathbf{f}(t)\}, \tag{1}$$

where the $n \times n$ mass, viscous damping, and stiffness matrices, [**M**], [**C**], and [**K**], describe the system near its nominal operating (equilibrium) point, P, $\{\mathbf{x}(t)\}$ is the $n \times 1$ response vector, and $\{\mathbf{f}(t)\}$ is the $n \times 1$ external excitation vector with m non-zero entries. The complex frequency

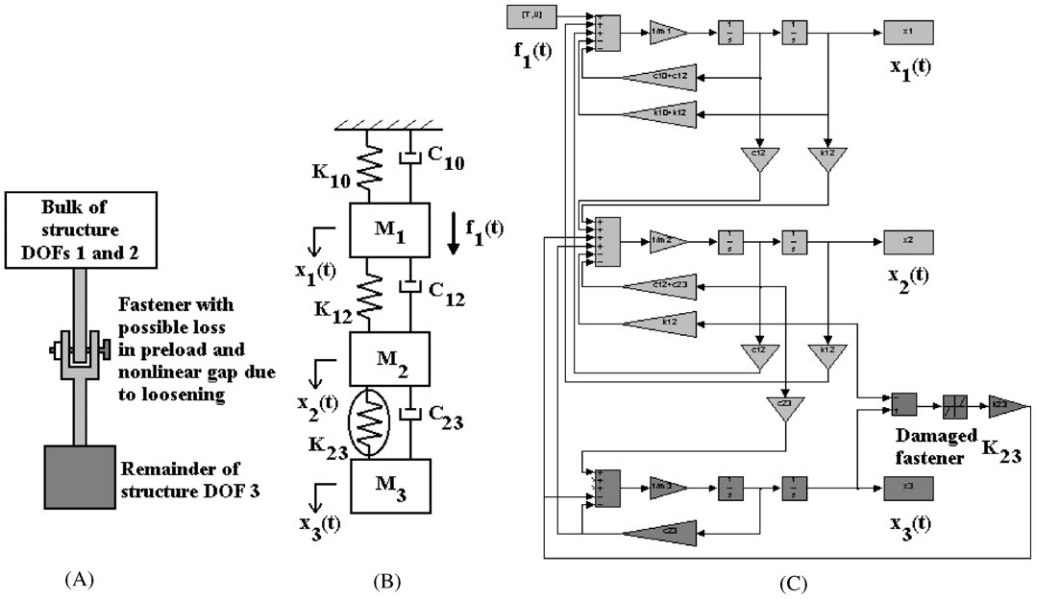

Fig. 3. (a) Physical system with bolted fastener, which can experience loss of preload and eventual non-linear clearance non-linearity; (b) corresponding 3-d.o.f. system with possible non-linear stiffness between d.o.f.s 2 and 3; (c) SIMULINK model.

domain version of Eq. (1) is

$$\begin{pmatrix} M_1 s^2 + (C_{10} + C_{12})s + K_{10} + K_{12} & -C_{12}s - K_{12} & 0 \\ -C_{12}s - K_{12} & M_2 s^2 + (C_{12} + C_{23})s + K_{12} + K_{23} & -C_{23}s - K_{23} \\ 0 & -C_{23}s - K_{23} & M_3 s^2 + C_{23}s + K_{23} \end{pmatrix} \times \{\mathbf{X}(s)\} = \{\mathbf{F}(s)\}, \quad [\mathbf{B}(s)]\{\mathbf{X}(s)\} = \{\mathbf{F}(s)\}, \tag{2}$$

where M_i is the ith lumped mass, and C_{jk} and K_{jk} are the viscous damping and stiffness, respectively, acting between the jth and kth d.o.f.s. Of course, in general the first and third d.o.f.s could also be coupled, but in many mechanical systems this assumption of nearest-neighbor coupling is valid (e.g., sparse sensor arrays placed across structural joints). The inverse of the system impedance matrix, $[\mathbf{B}(s)]$, is the transfer function matrix, $[\mathbf{H}(s)]$, which is derived below:

$$\{\mathbf{X}(s)\} = [\mathbf{B}(s)]^{-1}\{\mathbf{F}(s)\} = [\mathbf{H}(s)]\{\mathbf{F}(s)\},$$
$$[\mathbf{H}(s)] = \frac{1}{\Delta(s)} \begin{pmatrix} A_{11}(s) & A_{12}(s) & A_{13}(s) \\ A_{12}(s) & A_{22}(s) & A_{23}(s) \\ A_{13}(s) & A_{23}(s) & A_{33}(s) \end{pmatrix} = \begin{pmatrix} H_{11}(s) & H_{12}(s) & H_{13}(s) \\ H_{12}(s) & H_{22}(s) & H_{23}(s) \\ H_{13}(s) & H_{23}(s) & H_{33}(s) \end{pmatrix}, \tag{3}$$

where

$$A_{11}(s) = (M_2s^2 + (C_{12} + C_{23})s + K_{12} + K_{23})(M_3s^2 + C_{23}s + K_{23}) - (C_{23}s + K_{23})^2, \quad (4)$$

$$A_{12}(s) = (C_{12}s + K_{12})(M_3s^2 + C_{23}s + K_{23}), \quad (5)$$

$$A_{13}(s) = (C_{12}s + K_{12})(C_{23}s + K_{23}), \quad (6)$$

$$A_{22}(s) = (M_1s^2 + (C_{12} + C_{10})s + K_{10} + K_{12})(M_3s^2 + C_{23}s + K_{23}), \quad (7)$$

$$A_{23}(s) = (C_{23}s + K_{23})(M_1s^2 + (C_{12} + C_{10})s + K_{10} + K_{12}), \quad (8)$$

$$A_{33}(s) = (M_1s^2 + (C_{10} + C_{12})s + K_{10} + K_{12})(M_2s^2 + (C_{12} + C_{23})s + K_{12} + K_{23}) - (C_{12}s + K_{12})^2. \quad (9)$$

Each $A_{jk}(s)$ is the (j,k) entry of the adjoint matrix of the impedance matrix and $\Delta(s)$ is the characteristic polynomial or determinant. $\Delta(s) = 0$ is the characteristic equation that determines the modal frequencies, which are global properties of the system.

The (analytical) transmissibility between d.o.f.s 2 and 3 is given by $T_{32}(s) = X_3(s)/X_2(s)$ when the input is at d.o.f 1 as shown in Fig. 3(b). This expression is given below:

$$T_{32}(s) = \frac{X_3(s)}{X_2(s)} = \frac{A_{13}/\Delta(s)}{A_{12}/\Delta(s)} = \frac{(C_{12}s + K_{12})(C_{23}s + K_{23})}{(C_{12}s + K_{12})(M_3s^2 + C_{23}s + K_{23})} = \frac{C_{23}s + K_{23}}{M_3s^2 + C_{23}s + K_{23}}. \quad (10)$$

Note that even though the system is of order six with three complex conjugate modal frequencies, $s_{i,i+1} = \sigma_i \pm j\lambda_i$ for $i = 1, 3, 5$, the transmissibility feature, $T_{32}(s)$, is only of order two. Furthermore, $T_{32}(s)$ depends only on the coupling parameters associated with the fastener. Consequently, the measured transmissibility function, $T_{32}(j\omega)$, is an ideal feature for diagnosing damage in this particular bolted joint because it is both sensitive to the damage parameter(s) of interest (K_{23}, C_{23}) and of low order; in other words, it lies on the damage center manifold.

2.2. Transmissibility-based diagnostics—simulations

Assume the parameters of the 3-d.o.f. system for a healthy preload state in the fastener are as given in Table 1. Simulation parameters associated with the SIMULINK model shown in Fig. 3(c) are also given in the table. A fixed step fourth order Runge Kutta solver was used to

Table 1
System and simulation parameters

M_1, M_2, M_3 (kg)	1
C_{10}, C_{12}, C_{23} (N s/m)	10, 10.2, 10
K_{10}, K_{12}, K_{23} (N/m)	1000, 1200, 1200
f_1 (t) (normal distribution)	1.0 $N_{r.m.s.}$
Δt (s)	0.001
Blocksize (samples)	4096
N_{avg}	50
Percent overlap (%)	70

simulate the response of the 3-d.o.f. system to a broadband random input of Gaussian distribution. Simulations were carried out for two different damage scenarios. In the first scenario, the stiffness K_{23} was reduced from 1200 to 600 N/m in stages to model the behavior of the physical system for reductions in preload within the joint. In the second scenario, K_{23} was set to 600 N/m and a gap non-linearity of varying severity (0.01, 0.05, and 0.1 mm) was introduced into the system to describe the rattling that would take place if the preload vanished completely between d.o.f.s 2 and 3. Note that the numerical integration step size in SIMULINK was chosen small enough to achieve an accurate solution in spite of the discontinuous nature of this deadzone non-linearity.

Fig. 4 shows the effects on the magnitude of the transmissibility function, $T_{32}(j\omega) = X_3(\omega)/X_2(\omega)$, and the frequency response function (FRF), $H_{31}(j\omega) = X_3(\omega)/F_1(\omega)$, of varying the linear stiffness, K_{23}, associated with the preload in the joint. The results for four values of K_{23}, (-.-.-) 1188 N/m, (- - -) 1080 N/m, and (...) 600 N/m, are shown including the undamaged case, (—) 1200 N/m. Note that even though the FRF contains dynamics associated with all three d.o.f.s (sixth order), the transmissibility damage feature is of second order with only one discernible peak, which is reflected in Eq. (10). This reduction in dimensionality is a desirable characteristic in a damage detection feature as previously mentioned in Section 2.1. Also note that the transmissibility function is more sensitive than the FRF to the localized change in K_{23}. This increase in sensitivity to local changes in structures is also a desirable characteristic of a damage detection feature. As the preload is further reduced, the damage becomes non-linear in nature

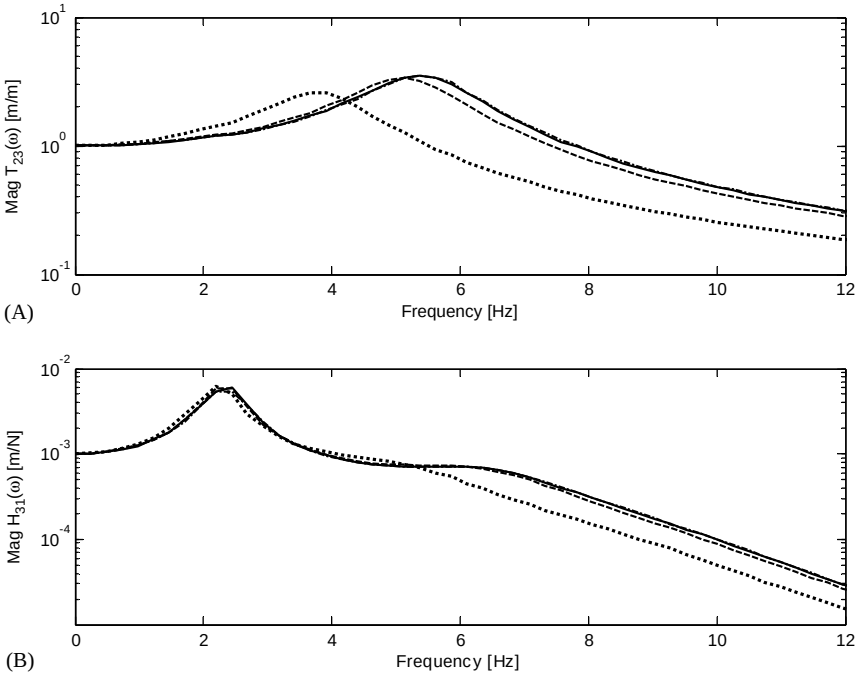

Fig. 4. (a) Transmissibility magnitudes between d.o.f.s 2 and 3 for reductions in K_{23} showing larger effects of loss in preload in bolted joint on the low order damage feature with legend: —, $K_{23} = 1220$ N/m (healthy); -.-.-, $K_{23} = 1188$ N/m; - - - , $K_{23} = 1080$ N/m; ..., $K_{23} = 600$ N/m; corresponding FRF magnitudes between input d.o.f. 1 and response d.o.f. 3.

according to the following form:

$$f_{n23}(x_3 - x_2) + K_{23} \cdot (x_3 - x_2 - \alpha) \quad \text{s.t.} \begin{cases} K_{23} = 600\,\text{N/m}, & -g > x_3 - x_2 > g, \\ \alpha = g(\text{or} - g), & |x_3 - x_2| > 0\,(\text{or} < 0), \\ K_{23} = 0\,\text{N/m}, & -g < x_3 - x_2 < g, \end{cases} \tag{11}$$

where f_{n23} is the non-linear restoring force within the gap between d.o.f.s 2 and 3. In the case of progressive non-linear damage, the transmissibility function continues to be a good indicator of the damage for varying gap sizes, (—) $g = 0$ mm, (-.-.-) $g = 0.01$ mm, (- - -)$g = 0.05$ mm, and (...) $g = 0.1$ mm, as shown in Fig. 5.

In order to quantify the differences that are visible in Figs. 4 and 5, the magnitudes of the ratios of damaged (linear and non-linear) to undamaged (i.e., linear with $K_{23} = 1200$ N/m) transmissibility functions are formed as shown in Fig. 6. The linear damage comparisons are indicated with (ooo) symbols and the non-linear damage comparisons with (xxx) symbols; the line types correspond to the three damage levels as before in both the linear and non-linear cases. Note that non-linear damage with the largest gap deviates the most from unity at all frequencies, which is expected because it corresponds to the most severe damage case. By rectifying these curves about unity as shown at the top of Fig. 7, and then integrating these rectified functions with frequency, the transmissibility-based diagnostic features at the bottom of Fig. 7 are obtained. The change in

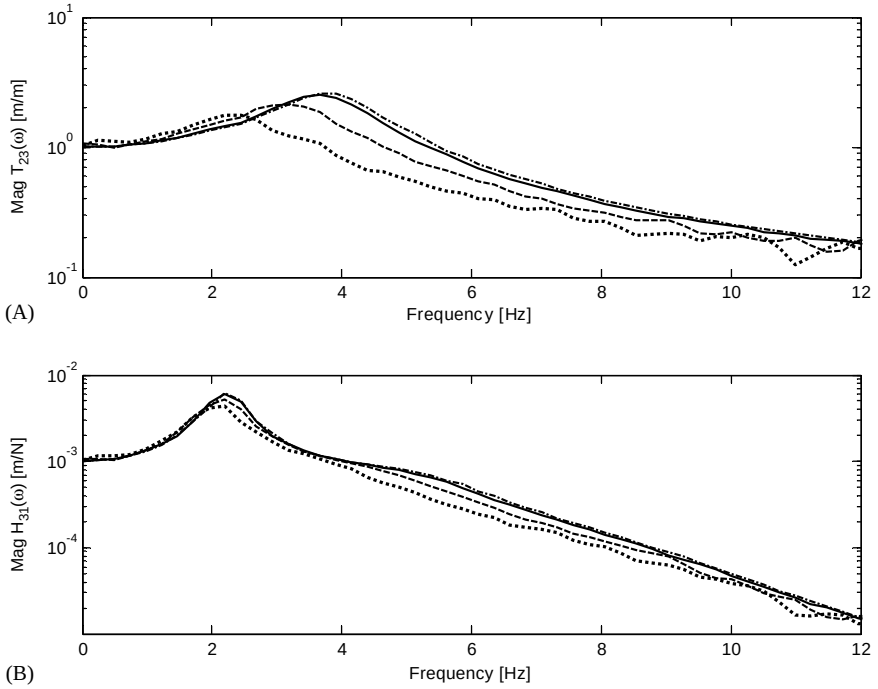

Fig. 5. (a) Transmissibilities magnitudes between d.o.f.s 2 and 3 for fixed $K_{23} = 600$ N/m showing large effects of growing gap non-linearity in bolted joint on the low order damage feature with legend: —, $g = 0$ mm; -.-.-, $g = 0.01$ mm; - - -, $g = 0.05$ mm; ..., $g = 0.1$ mm; (b) corresponding FRF magnitudes between input d.o.f. 1 and response d.o.f. 3.

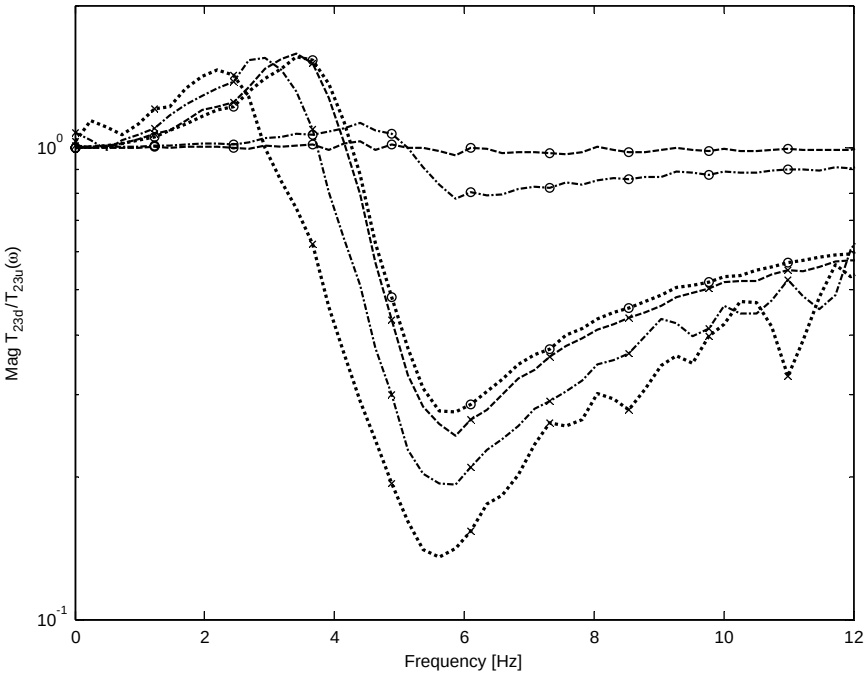

Fig. 6. Magnitudes of ratios of transmissibilities from Figs. 4 and 5 between damaged and undamaged (linear, $K_{23} = 1200$ N/m) cases with same legend as in those figures and: ooo, linear damage; xxx, non-linear damage.

magnitudes of these integrals within a baseband frequency range is the feature of interest in the remainder of this work. Experiments are carried out on a rotorcraft fuselage in Section 4 using this transmissibility-based integral feature.

3. Equilibrium point damage models

3.1. Models for damage accumulation

'Damage' is a complicated phenomenon. By definition, damage varies from zero in a healthy system or structure to unity when failure occurs [26]. Structural damage can occur when components fatigue after many cycles (hard failure due to overuse) or during a break-in period (soft failure due to design flaw). For instance, a structure becomes damaged if a rivet/bolt fails or if a flaw evolves into a crack. Regardless of whether a structure is homogeneous or heterogeneous in nature, damage phenomena always involve temporal (e.g., number of cycles, time under mild/severe operation) and spatial (e.g., fastener location, site of crack initiation) characteristics. The same can be said of experimental structural dynamic measurements, which involve sensors, actuators, and measurement d.o.f.s with temporal (time/frequency) and spatial (location/direction) characteristics. Although different kinds of damage (e.g., cracks, fastener failures, delamination) are governed by different physical models, the experimental process of extracting

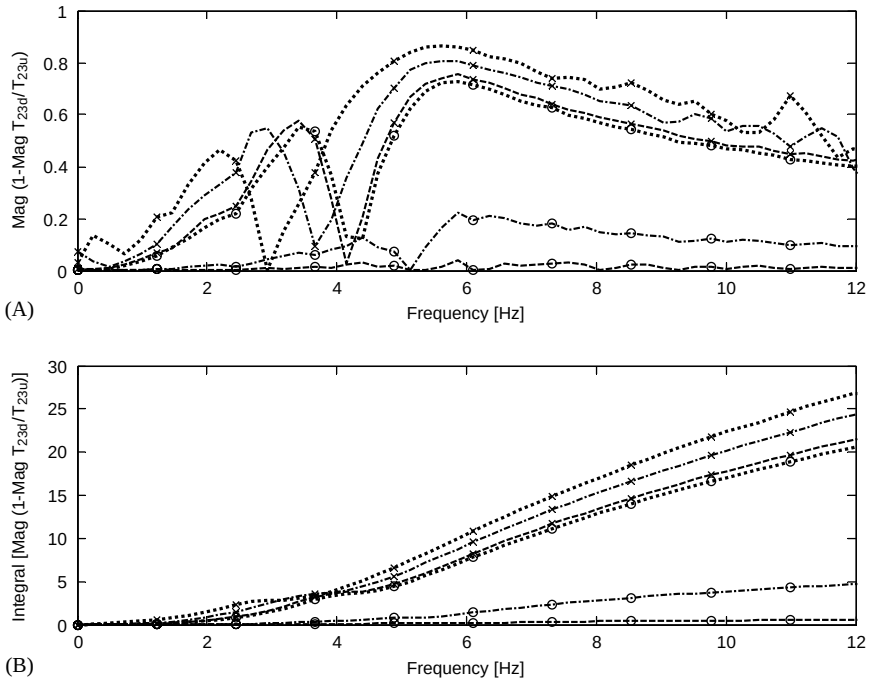

Fig. 7. (a) Rectified version of Fig. 6 about unity; (b) frequency-wise integral of the result in the top plot indicating the most severe damage with complete loss of preload and introduction of $g = 0.1$ mm gap non-linearity.

features from input–output data, which can be used to quantify the accumulation of damage, is largely independent of the particular application.

The purpose of on-line damage prognosis is to model (or trend) damage evolution, taking into account specialized physics and constitutive laws only if necessary. Predictions about remaining life can then be made. Damage prognosis algorithms like the one describe here are being designed for SHM installations in transportation and defense-related systems (e.g., composite armor) [1]. The technique here models the change in the transmissibility-based diagnostic feature from Section 2 with a low order non-linear dynamic equation. Fig. 2 illustrated two examples of this kind of bifurcation. Assume the progression of damage in the cracked plate shown in the figure is diagnosed using the normalized crack length as a damage variable, X. Under mild operating conditions, the crack opens and closes frequently depending on the input, but only grows in a quasi-stationary manner along the path from point 1 to point 2; however, the crack may rapidly tear if the operating conditions are severe enough (see path from point 3 to point 4). The cusp catastrophe along this path describes a codimension two bifurcation; two variables, the operating severity, A, and the time in service, B, determine how damage evolves along the surface. The simple first order equation,

$$\dot{X} = B + AX - X^3, \tag{12}$$

describes the evolution of real equilibrium (stationary) points, X_e, along this surface. Only the real equilibria are of interest here because diagnostic features are real numbers. This equation is called

a normal form; other types of normal forms describing transcritical, saddle node (blue sky), and super- and subcritical pitchfork bifurcations also appear frequently in the literature [17, 27–30].

The important point to make here is that a low order non-linear dynamic model like the one in Eq. (12) can be used to model complicated damage processes. As a structural dynamic system, like the one illustrated in Fig. 3, operates, its damage state moves along the manifold of equilibrium points. At each state, the rate at which damage will accumulate is determined by the location of the equilibrium point on the manifold. For example, many different structural components in aircraft (e.g., wing, spar, fuselage) have been shown to exhibit first order damage-to-residual life relationships similar to the one shown in Fig. 2 [31]. Furthermore, Song and Bae [32] have produced data that follows a first order relationship between crack length (i.e., damage variable) and crack propagation rate (slope of damage manifold) as have Cowie [33], Dawicke et al. [34], and Broede and Koehl [35] in the context of damage tolerant design. In addition, Lachmann et al. [36], Daniel and March [37], and others have demonstrated similar relationships in metal fasteners and structural composite layers (glass/epoxy laminate), respectively. Of course, these processes are usually statistically uncertain, so Eq. (12) should be accompanied by some sort of probability distribution assumptions to be useful in practice.

Although Eq. (12) is an example of a reasonable model to propose for damage prognosis, Daniel points out that damage at the microscopic level is really best represented by a tensorial quantity [37]. Because the SHM development here makes the assumption that a feature for diagnosing damage is observable (see Section 1.2), and because most sensors are not tensorial in nature, scalar damage theory is assumed to be valid. In any event, this assumption is associated with experimental observability of the evolution of damage.

3.2. Non-linear bifurcations in damage evolution

The meaning of Eq. (12) can be extracted from the theory of imperfection bifurcations. This theory examines the bifurcation diagrams of dynamic systems like the one in Eq. (12) for fixed A with variable B and then for fixed B with variable A, respectively. Physically, these two different scenarios with A and B mean that the evolution of the damage equilibrium variable, X_e, is first studied as time elapses by fixing the operating severity, and is then studied for variable operating severity at a fixed number of cycles. Fig. 8 shows the results of each of these analyses overlayed on top of the equilibrium damage manifold (i.e., X_e versus A and B). For example, the right plot in the figure shows the one-dimensional plot of X_e versus A for $B=0$ and the left plot shows one-dimensional plots of X_e versus B for $A<0$ and $A>0$. These equilibrium bifurcation diagrams are physically meaningful. For instance, for $A<0$ (less severe operating environment) the damage accumulates gradually as shown; however, for $A>0$ (more severe operating environment) the damage gradually accumulates until the hilltop on the manifold is reached beyond which the damage suddenly worsens. Physical quantities A, B, and X_e must be normalized to match the dimensionless axes shown in Fig. 8. At each point on the surface, X_e, the rate at which damage is accumulating can be estimated from Eq. (12). This rate of accumulation is the 'prognostic' shown in Fig. 1. The prognostic can then be used for life prediction in a given operating environment or set of operating environments.

Although Eq. (12) is a suitable model for describing damage evolution using normal forms, experimental data from high order systems may first have to be reduced in dimension before

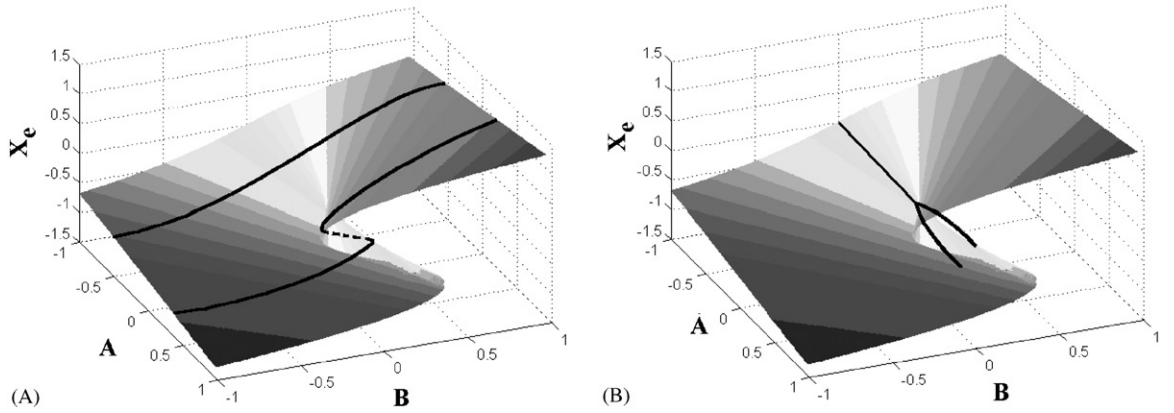

Fig. 8. (a) Surface plot of real equilibrium points showing two saddle node bifurcations and (b) equilibrium surface plot showing supercritical pitchfork bifurcation.

applying this prognosis model. There are two ways to do this: (1) center manifold theory [16] and (2) feature extraction [38]. Center manifold theory provides the means to do dimensionality reductions in general by dividing the spectrum of a structural dynamic system into stable, unstable, and center eigenspaces (i.e., Re $\lambda<0$, Re $\lambda>0$, Re $\lambda=0$, respectively) via a modal transformation [39]. Once this transformation is accomplished, the theory ensures that bifurcations (damage evolution) occur along the center manifolds (i.e., hypersurfaces governed by principal co-ordinates associated with the centers only). Furthermore, the theory of normal forms guarantees that a complicated center manifold equation can be simplified into normal forms similar to Eq. (12) [29,30]. Unfortunately, experimental data involving all the states, which are needed to apply analytical center manifold reductions, is usually not available.

Feature extraction is the alternative, more empirical, data reduction technique employed here. By acquiring data and then compressing it as in Section 2 using transmissibility estimates, low order damage features can be extracted from high order structural dynamic measurements. Recall from Section 1.2 the assumption here that a diagnostic feature can be selected from available data to achieve the desired degree of dimensionality reduction. To that end, the analytical/simulation results in Section 2 showed that transmissibility-based diagnostic features can be selected to provide a low-dimensional quantitative description of damaged structures. In fact, the integral feature at the bottom of Fig. 7 is a second order function of the coupling stiffness/damping (linear and non-linear) between d.o.f.s 2 and 3. This assumption is also justified experimentally in Section 4. In summary, features like the transmissibility-based indicators in Section 2 can often be selected to reduce the dimension of diagnostic processes, so center manifold theory may not be needed.

Before proceeding to describe the experimental results, consider the possible physical variables associated with the mathematical parameters A and B in Eq. (12). The discussion above made the associations $A\leftrightarrow$ operating severity and $B\leftrightarrow$ time in operation; however, different features may be more or less sensitive to the damage. For instance, transmissibility estimates between a certain pair of d.o.f.s might exhibit a sudden change indicative of the cusp in the left plot of Fig. 8 whereas a transmissibility function between a different pair of d.o.f.s may exhibit the gradual

changes shown in that plot. This association $A \leftrightarrow$ spatial feature location is also experimentally meaningful and is discussed below.

4. Experiments

4.1. Experimental set-up

A series of experiments was conducted on the Bell 206L fuselage in Fig. 9. The fuselage is $18' \times 7' \times 7'$ without the gearbox or rotor and is of aluminum construction. It possesses many components that are typical in structures on which damage is observed including a structural box frame, overlapping fuselage skin, and several kinds of fasteners (e.g., rivets, bolts, etc.). A 16-channel 51.2 kHz Agilent VXI data acquisition system was used to acquire uniaxial acceleration response measurements at six hinge locations along the side of the fuselage (Fig. 10). The measurements were taken on the hinges in the direction of the bolt axes. A 50 lb MB Dynamics electrodynamic shaker was attached at the base of the fuselage and driven with a 10 to 2000 Hz broadband random excitation time history. A relatively high frequency range was used to observe the local damage of interest in the bolted joints because this type of local damage does not significantly affect global (low-frequency) modes of vibration. Furthermore, it was desired to detect very small changes in preload in the joint, so a higher frequency excitation produced shorter wavelength vibrations, which were capable of detecting relatively small changes in the bolt. It should also be noted that typical operating input frequencies in the fuselage (e.g., gear train) are also in that range.

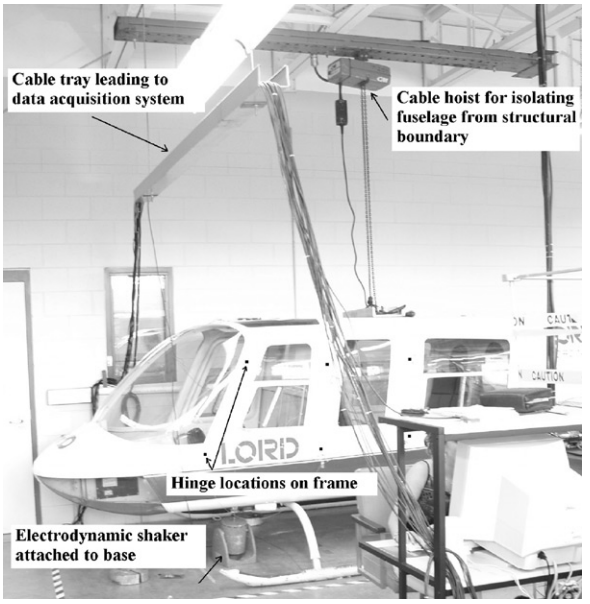

Fig. 9. Rotorcraft fuselage supported with hoist.

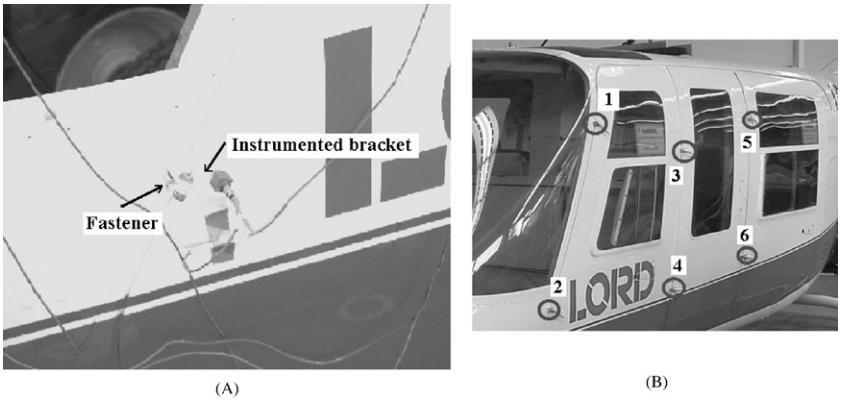

Fig. 10. (a) Rotorcraft fuselage bracket with fastener and (b) measurement d.o.f.s at hinge locations.

The fuselage hinges were instrumented with 100 mV/g (nominal sensitivity) PCB piezoelectric shear mode accelerometers using a thin layer of wax. The bandwidth for the measurements was 12.8 kHz and the number of samples per channel was 2^{17}. Long time histories were desirable because overlap signal processing was used to estimate the transmissibility functions as described below. Fig. 11 shows the magnitude and phase (unwrapped) of two different FRFs between the input d.o.f. at the base of the fuselage and acceleration response measurements at d.o.f.s 1 and 3 in Fig. 10 (right). These two measurement d.o.f.s were located on different brackets on different compartment panels.

4.2. *Diagnosis and prognosis using transmissibility*

The transmissibility feature used to diagnose damage was the integral of 1-Mag $(T_d(\omega)/T_u(\omega))$, where $T_d(\omega)$ and $T_u(\omega)$ are the transmissibilities in the damaged and undamaged systems, respectively. $T_d(\omega)$ and $T_u(\omega)$ were estimated using standard H_1 FRF estimation techniques with 50% overlap processing, 10 averages, and 2048 blocksizes. Data from the undamaged and various damaged cases were analyzed sequentially to examine how the diagnostic feature would change if damage of the type and severity imposed was experienced in near real-time. The reversible damage was imposed by loosening a bolt at a single hinge in three stages: slight, moderate, and full reduction in preload of the bolt. Transmissibility functions were estimated from response measurements between the sensor at the damaged fastener bracket and sensors at the other five brackets.

Fig. 12 shows the magnitude and phase plots for transmissibility functions between d.o.f.s 1 and 2 in the healthy structure (—) and in the most severe damage state (...) involving the complete loosening of the bolt in the hinge at d.o.f. 1. Note that the loosened bolt has caused the peaks in the transmissibility plot to shift downward in frequency similar to the simulation results in Figs. 4 and 5; the same downward shifts occur in the slight and moderate preload reduction damage states as well. The integrated near real-time diagnostic indicators associated with these transmissibility functions are shown in Fig. 13 for three different pairs of d.o.f.s. In d.o.f. pair 1–3 (xxx), there are two significant steps down in the diagnostic corresponding to the initially mild

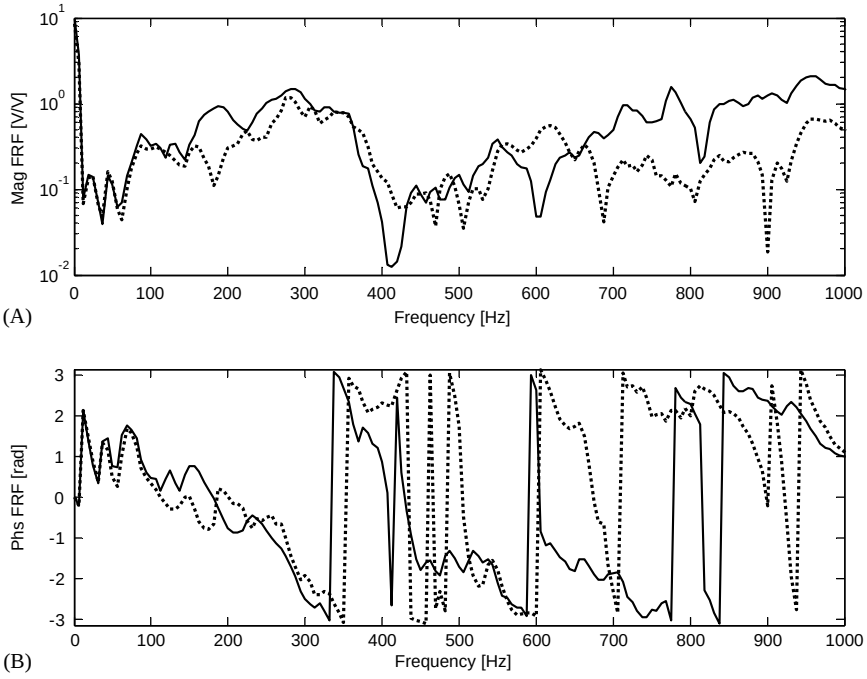

Fig. 11. (a) Magnitude plots of FRFs between input d.o.f. and response d.o.f.s 1 and 3 for healthy structure in helicopter fuselage; (b) phase plots with legend:—, FRF from input to d.o.f. 1; ... , FRF from input to d.o.f. 3.

and then moderate preload reductions, and then a gradual change in the indicator occurs between the moderate and severe damage cases. In d.o.f. pair 1–2 (ooo), there is only one significant step down in the indicator corresponding to the first applied mild damage case. Lastly, in d.o.f. pair 3–4 (+ + +), there is a gradual trend downward in the indicator for progressive damage in d.o.f. 1 but no obvious steps occur.

The differences between these d.o.f. pairs stems from their different structural interconnectivities (see right, Fig. 10) in relation to the damage location at d.o.f. 1. D.o.f. pair 1–3 extends from one panel with the damaged fastener to an undamaged panel, d.o.f. pair 1–2 spans the single panel with a damaged fastener, and d.o.f. 3–4 spans a single panel without a damaged fastener. The damage was introduced at cycle numbers 6, 18, and 33. Similar results and conclusions can be made from Fig. 14, which shows results of the near real-time integral transmissibility-based damage indicator for a fastener on a different panel at d.o.f. 3 in Fig. 10. Note that the pairs involving d.o.f. 3 in this case exhibit the most significant steps at each progressive damage state (cycles 6, 25, and 30).

The results in Figs. 13 and 14 show that even though the fuselage possesses many modes of vibration (i.e., it is of high order), which are evident in the FRFs in Fig. 11, in the frequency range of interest, the damage indicator associated with each d.o.f. pair evolves on a low order surface similar to the one in Fig. 8. This low order surface was referred to as the damage center manifold in Section 3. By modelling the damage indicator (diagnostic) with a low order normal form bifurcation model similar to the one in Eq. (12), the resultant model can be used to predict when

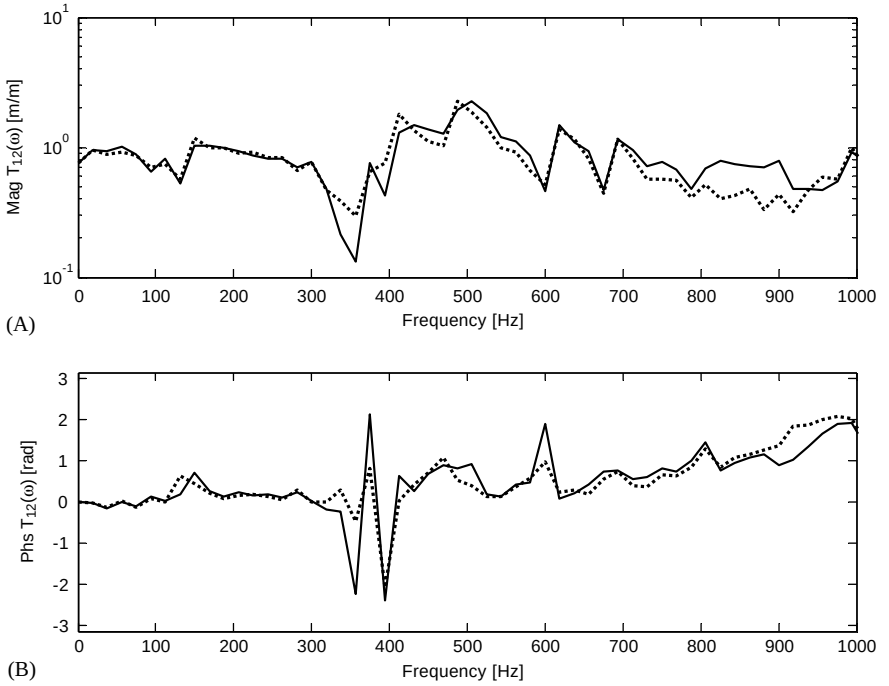

Fig. 12. (a) Magnitude plots of transmissibilities between d.o.f.s 1 and 2 for healthy structure and loosened fastener in helicopter fuselage; (b) phase plots with legend: (—) health and (...) unhealthy.

sudden changes (bifurcations) in structural health are about to occur or when changes will be gradual instead. Figs. 13 and 14 clearly illustrate both of these types of changes.

For example, Fig. 15 shows the results for damage of varying severity at the second hinge at d.o.f. 2 in Fig. 10. These results are presented in a different format than in the previous figures. Note that each pair of d.o.f.s (1–2, 1–3, etc.) exhibits a different type of damage evolution and that the surface of transmissibility-based diagnostics closely resembles that of the normal form imperfection bifurcation in Eq. (12). The ordering of the d.o.f. pairs on the x-axis was determined by placing them in order of their increasing distance from the damaged fastener. This ordering is what caused the indicator to take the form of an asymmetrical pitchfork bifurcation.

This manifold of damage equilibrium points can be used to trend the transmissibility-based diagnostics to carry out near real-time damage prognosis. The following first-order normal form equation describes the damage manifold in the left of Fig. 15:

$$\dot{X}_{DI} = B_{TIO} + A_{DOFP} X_{DI} - X_{DI}^3, \tag{13}$$

in which X_{DI} denotes the damage indicator or feature of interest (transmissibility in this case), $X_{e,\ DI}$ are the equilibria or damage states on the damage manifold of diagnostic features, B_{TIO} is the (normalized) time in operation, and $A_{d.o.f.P}$ is the (normalized) d.o.f. pair for comparison. By modelling the evolution of transmissibility-based diagnostic features with Eq. (13), the bifurcations and smooth transitions of damage can be assessed and possibly even predicted. In other words, the model is a valid tool for damage prognosis. Of course, the model is more

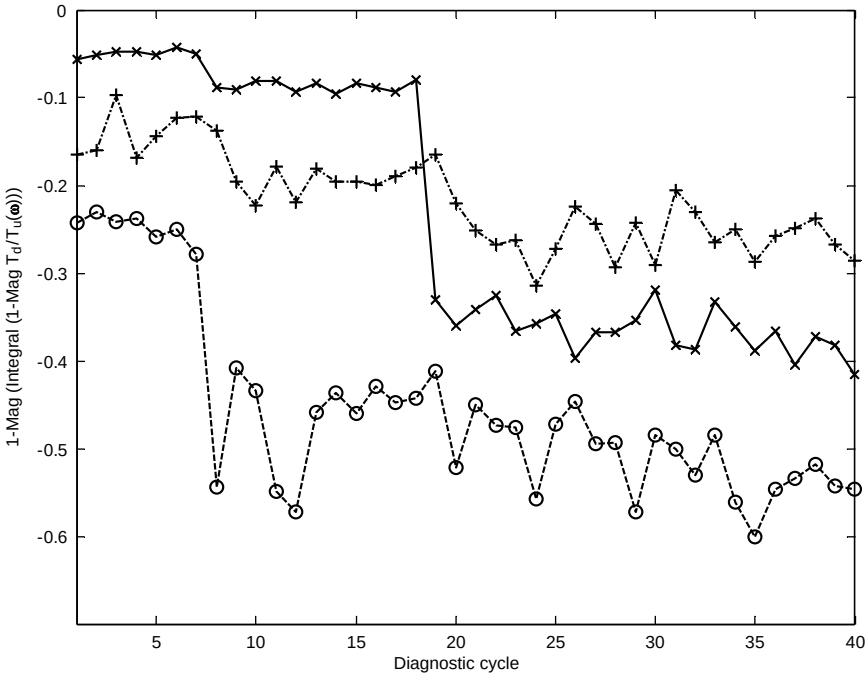

Fig. 13. Transmissibility-based damage indicators in near real-time for progressively damaged fastener at d.o.f. 1 at cycles 6, 18, and 33 in a helicopter fuselage with legend: xxx, d.o.f. pair 1–3; ooo, d.o.f pair 1–2; + + +, d.o.f. pair 3–4.

valuable if the steps or bifurcations are found a priori so that critical times of operation can be determined. It is important to note again that Eq. (13) was phenomenologically motivated; it was not derived from first principles, which is one of the primary areas for future work. Also note that the research here focused on damage prognosis as it related to the transitions in the damage indicators; however, the use of multiple time scales for describing the slow evolution of structural damage is also being addressed elsewhere by the authors.

5. Conclusions

This paper described a method for modelling certain kinds of damage evolution in distributed mechanical structures using non-linear normal forms. First, a diagnosis technique based on transmissibility functions between pairs of d.o.f.s was discussed as a means for extracting low order features from high order experimental structural dynamic data. It was demonstrated analytically that these diagnostic features are sensitive to linear and non-linear types of damage (e.g., losses in preload and gap non-linearities, for example). Next, the damage prognosis model was introduced in the context of a typical first order non-linear dynamic system, which possessed equilibrium points that generated a manifold in a two-dimensional parameter space. Different types of damage/failures that exhibit this type of low order behavior were cited from the experimental mechanics literature. Lastly, dynamic experiments on a rotorcraft fuselage were conducted to diagnose varying levels of damage in fasteners on fuselage panels. It was shown that

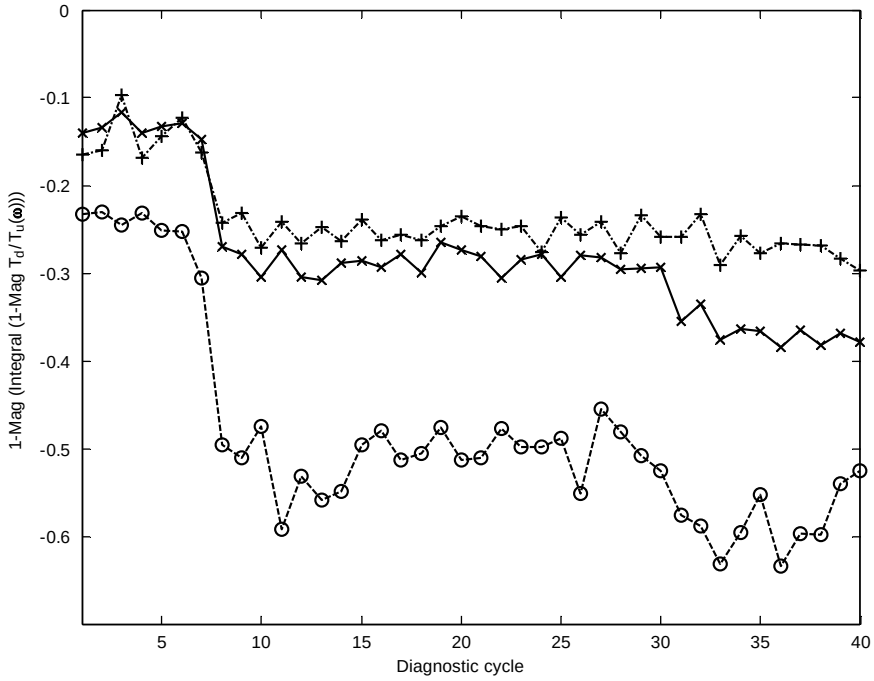

Fig. 14. Transmissibility-based damage indicators in near real-time for progressively damaged fastener at d.o.f. 3 at cycles 6, 25, and 30 in a helicopter fuselage with legend: xxx, d.o.f. pair 3–4; ooo, d.o.f pair 3–4; + + +, d.o.f. pair 2–6.

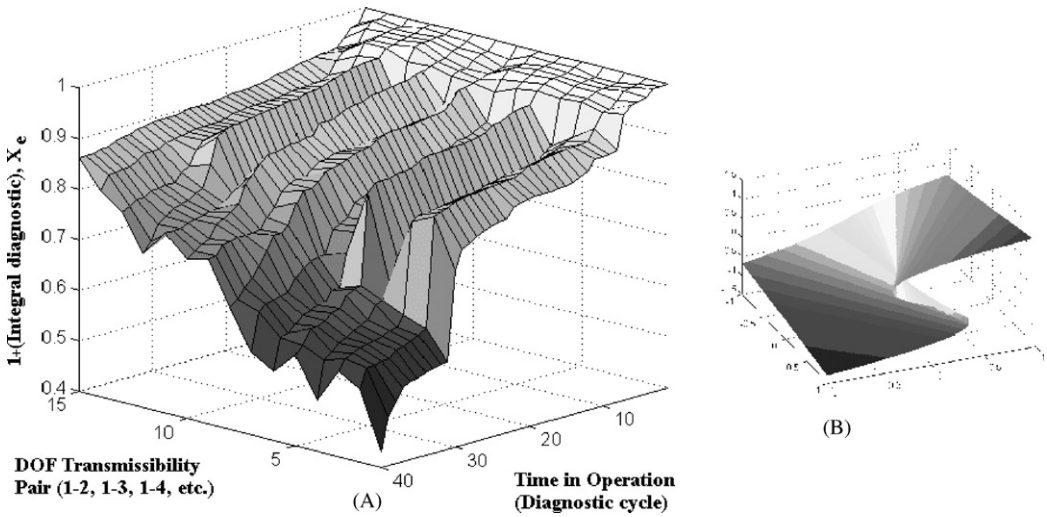

Fig. 15. Damage 'center' manifold (a) of fuselage at second fastener, d.o.f. 2, showing similarity to the low order equilibrium point surface (b) of model in Eq. (12).

the indicators moved along a surface similar to the manifold of equilibrium points in a first order cubic differential equation. The resulting prognosis models were functions of temporal (e.g., time in operation) and spatial bifurcation parameters (e.g., d.o.f. pair). Future work will apply these

models in experimental SHM and NDE applications involving multiple types of damage in heterogeneous structures (e.g., laminated composite armor, composite rocket motor cases, etc.).

Acknowledgements

The authors gratefully acknowledge the Department of the Army, Army Research Office for their support of this work under grant DAAD19-02-1-0185 with Dr. Gary Anderson as program manager, the Office of Science and Technology Policy for confirming the Department of Defense nomination of the author for a 2001 Presidential Early Career Award for Scientists and Engineers, Dr. L. Miller of Lord Corporation and M. Lally of The Modal Shop of PCB Group for making the fuselage and sensors available, respectively, for use in these experiments, and Profs. Singh and Selamet for their invitation to participate in the India–USA Workshop on Experimental Structural Dynamics.

References

[1] C. Farrar (Organizer), Damage Prognosis Workshop, March 2001, spons. by Los Alamos National Latoratory, Phoenix, AZ.
[2] J.N. Schoess, Conductive polymer sensor arrays: a new approach for structural health monitoring, Proceedings of the International Society of Optical Engineering, Advanced Nondestructive Evaluation for Structural and Biological Health Monitoring, Vol. 4335, 2001, pp. 9–19.
[3] J.D. Achenbach, D.O. Thompson, Towards quantitative non-destructive evaluation of aging aircraft, in: S.N. Atluri, S.G. Samrath, P. Tong (Eds.), Structural Integrity of Aging Airplanes, Springer, Berlin, 1991, pp. 1–13.
[4] E. White, in: C. Farrar (Organizer), Damage Prognosis Workshop, March 2001, spons. by Los Alamos National Laboratory, Phoenix, AZ.
[5] S.M. Walsh, J.C. Butler, J.H. Belk, R.A. Lawler, Development of a structurally compatible sensor element, Proceedings of the International Society of Optical Engineering, Advanced Nondestructive Evaluation for Structural and Biological Health Monitoring, Vol. 4335, 2001, pp. 63–73.
[6] T.E. Baker, Condition monitoring innovations for U.S. army rotorcraft, Proceedings of the Second International Workshop on Structural Health Monitoring, Stanford, CA, September 1999, pp. xix–xxix.
[7] T.L. Vandiver, Health monitoring of U.S. Army Missile Systems, Proceedings of the International Workshop on Structural Health Monitoring, Stanford, CA, September 1997, pp. 191–196.
[8] J.D. Cronkhite, L. Gill, (Technical evaluators), RTO AVT Specialists' Meeting on Exploitation of Structural Loads/Health Data for Reduced Life Cycle Costs, Brussels, Belgium, "RTO MP-7", 1998.
[9] S.W. Doebling, C.R. Farrar, M.B. Prime, D.W. Shevitz, Damage identification and health monitoring of structural and mechanical systems from changes in their vibration characteristics: a literature review, Los Alamos Report LA-13070-MS, 1996.
[10] J. Lemaitre, Local approach of fracture, Engineering Fracture Mechanics 25 (5,6) (1986) 523–537.
[11] K.C. Chang, T.K. Lin, Y.B. Lin, L. Wang, FBG sensors for structural health monitoring, Proceedings of the International Society of Optical Engineering, Advanced Nondestructive Evaluation for Structural and Biological Health Monitoring, Vol. 4335, 2001, pp. 35–42.
[12] J. Matrat, K. Levin, R. Jarlas, Effect of debonding on strain measurement of embedded Bragg grating sensors, Proceedings of the International Workshop on Structural Health Monitoring, Stanford, CA, September 1999, pp. 651–660.
[13] P. Blanas, M.P. Wenger, R.J. Shuford, K.K. Das-Gupta, Active composite materials and damage monitoring, Proceedings of the International Workshop on Structural Health Monitoring, Stanford, CA, September 1997, pp. 199–207.

[14] P. Blanas, E. Rigas, D.K. Das-Gupta, Health monitoring of composite structures using composite piezoelectric transducers, in: F.K. Chang (Ed.), Proceedings of the International Workshop on Structural Health Monitoring, Stanford, CA, September 1999, pp. 635–642.
[15] C.S. Wang, F.K. Chang, Built-in diagnostics for impact damage identification of composite structures, in: F.K. Chang (Ed.) Proceedings of the International Workshop on Structural Health Monitoring, Stanford, CA, September 1999, pp. 612–621.
[16] J. Guckenheimer, P. Holmes, Nonlinear Oscillations, Dynamical Systems, and Bifurcations of Vector Fields, Applied Mathematical Sciences, Vol. 42, Springer, New York, 1983.
[17] S.H. Strogatz, Nonlinear Dynamics and Chaos, Addison-Wesley, Reading, MA, 1994.
[18] H.P. Bloch, F.K. Geitner, Machinery Failure Analysis and Troubleshooting, Gulf Publishing Company, Houston, TX, 1994.
[19] W.R. Buckland, Statistical Assessment of the Life Characteristic: A Bibliographic Guide, Hafner, New York, 1964.
[20] L.J. Hart-Smith, Nonlinear analysis of bonded/bolted joints, Design Methodology for Bonded-Bolted Composite Joints, Analysis Derivations and Illustrative Solutions, Part 4, Douglas Aircraft Company, USAF Flight Dynamics Laboratory, 1988.
[21] L.J. Hart-Smith, Adhesive bond stresses and strains at discontinuities and cracks in bonded structures, Journal of Engineering Materials and Technology 100 (1978) 16–24.
[22] C.E. Witherell, Mechanical Failure Avoidance: Strategies and Techniques, McGraw-Hill, New York, 1994.
[23] F.C. Moon, Nonlinear system identification and control of fluid-elastic vibrations using bifurcation theory, Experimental Nonlinear System Identification Workshop, NASA Langley Research Center, Hampton, VA, May 2001, 1980.
[24] N.S. Namachchivaya, Co-dimension two bifurcations in the presence of noise, Journal of Applied Mechanics 58 (1) (1991) 259–265.
[25] T.J. Johnson, D.E. Adams, Transmissibility as a differential indicator of structural damage, ASME Journal of Vibration and Acoustics 124 (2002) 634–641.
[26] S. Murakami, Mechanical modeling of material damage, Journal of Applied Mechanics 55 (1988) 280–286.
[27] E.A. Jackson, Perspectives of Nonlinear Dynamics, Vol. 1, Cambridge University Press, Cambridge, UK, 1989.
[28] A.H. Nayfeh, B. Balachandran, Applied Nonlinear Dynamics: Analytical, Computational, and Experimental Methods, Wiley, New York, 1995.
[29] A.H. Nayfeh, Method of Normal Forms, Wiley, New York, 1993.
[30] P.B. Kahn, Y. Zarmi, Nonlinear Dynamics Exploration through Normal Forms, Wiley, New York, 1998.
[31] C. Boller, C. Biemans, Structural health monitoring in aircraft-state-of-the-art, perspectives and benefits, Proceedings of the Second International Workshop on Structural Health Monitoring, Stanford, CA, September 1999, pp. 541–552.
[32] S.H. Song, J.S. Bae, Fatigue crack initiation and propagation from hole defects, Experimental Mechanics, Society for Experimental Mechanics 38 (3) (1998) 161–166.
[33] W.D. Cowie, A damage tolerance approach for management of aging gas turbine engines, in: S.N. Atluri, S.G. Samrath, P. Tong (Eds.), Structural Integrity of Aging Airplanes, Springer, Berlin, 1991, pp. 100–114.
[34] D.S. Dawicke, C.C. Poe, J.C. Newman, C.E. Harris, An evaluation of the pressure proof test concept for 2024-T3 aluminum alloy sheet, in: S.N. Atluri, S.G. Samrath, P. Tong (Eds.), Structural Integrity of Aging Airplanes, Springer, Berlin, 1991, pp. 115–129.
[35] J. Broede, M. Koehl, Aero engine life usage monitoring including safe crack propagation, Proceedings of the International Workshop on Structural Health Monitoring, Stanford, CA, September 1999, pp. 142–152.
[36] C. Lachmann, Th. Nitschke-Pagel, H. Wohlfahrt, Nondestructive characterization of fatigue processes in cyclically loaded welded joints by the Barkhaussen noise method, in: Proceedings of the International Workshop on Structural Health Monitoring, Stanford, CA, September 1999, pp. 327–336.
[37] I.M. Daniel, Experimentation and modeling of composite materials, 1998 William M. Murray Lecture, Experimental Mechanics, Society for Experimental Mechanics 39 (1) (1999) 1–19.
[38] C.M. Bishop, Neural Networks for Pattern Recognition Clarendon Press, Oxford, 1995, p. 295 (Chapter 8).
[39] D.E. Adams, Analytical and experimental coordinate transformations for high order structural dynamic systems, Proceedings of the International Modal Analysis Conference, Los Angeles, CA, February, 2002.